Journal of Solid State Chemistry 192 (2012) 273–283

Contents lists available at SciVerse ScienceDirect

Journal of Solid State Chemistry

journal homepage: www.elsevier.com/locate/jssc

A study of the crystal structures and the phase transitions of the ordered double perovskites Sr_2ScSbO_6 and Ca_2ScSbO_6

A. Faik [a,b,*], D. Orobengoa [c], E. Iturbe-Zabalo [a], J.M. Igartua [a]

[a] Fisika Aplikatua II Saila, Zientzia eta Teknologia Fakultatea, Euskal Herriko Unibertsitatea, P.O.Box 644, Bilbao 48080, Spain
[b] CICenergigune, Parque Tecnológico, Albert Einstein 48, 01510 Miñano, Álava, Spain
[c] Departamento de Física de la Materia Condensada, Universidad del País Vasco, E-48080 Bilbao, Spain

ARTICLE INFO

Article history:
Received 29 December 2011
Received in revised form
11 April 2012
Accepted 12 April 2012
Available online 24 April 2012

Keywords:
Double perovskite
X-ray and neutron powder diffraction
Crystal structure
Phase transitions
Symmetry adopted modes

ABSTRACT

The crystal structures and phase transitions of the two ordered double perovskites Sr_2ScSbO_6 and Ca_2ScSbO_6 were studied using conventional X-ray and neutron powder-diffraction methods. The crystal structures of both compounds have the $P2_1/n$ space group symmetry at room temperature, resulting from Sc/Sb ordering. The evolution with temperature of the structure of the Sr containing compound shows the presence of three phase transitions with the following sequence: $P2_1/n \rightarrow I2/m \rightarrow I4/m \rightarrow Fm\bar{3}m$, at about 400, 560 and 650 K, respectively. The smaller size of Ca cation, with respect to that of Sr cation, leads to a large distortion of Ca_2ScSbO_6 at room temperature. This fact in turn causes that the Ca containing compound shows only the first phase transition from $P2_1/n$ to $I2/m$ at high temperature at about 1440 K. The analysis of the phase transitions and the refinements have done using the symmetry-adapted modes and the tools of the Bilbao Crystallographic Server.

1. Introduction

The perovskite structure type is one of the most regularly observed structure types in condensed matter sciences and in advanced materials research and applications, as well. This is due to the wide array of properties it shows like superconductivity and magnetoresistance [1–3]. The double perovskite with general formula $A_2BB'O_6$ can be represented as a three-dimensional network of alternating BO_6 and $B'O_6$ octahedra, with A-atoms occupying the interstitial spaces between the octahedra. They constitute an important class of materials, characterized by subtle structural distortions from the cubic ($Fm\bar{3}m$, No. 225) prototype structure. The distortions are caused by rotations of the B O_6 and $B'O_6$ octahedra (tilts) with respect to the crystallographic axes of the material, to accommodate the size of the A-site cations.

Recently, the strontium antimony oxide compounds with double perovskite structure have attracted considerable attention [3–11]. In our previous works [12–16], we have studied the structures at room temperature and the possible phase transitions at low and high temperature for several compounds of this family. The study of phase transitions at low and high temperature is very important to understand the physical properties of these materials.

To complete these studies, we have focused our attention on other two members of this family: Sr_2ScSbO_6 and Ca_2ScSbO_6. To the best of our knowledge, this is the first time that the room-temperature structures of Sr_2ScSbO_6 and Ca_2ScSbO_6 are reported. Syntheses of Sr_2ScSbO_6 have been reported on two occasions [7,17]; however, no structural determination was reported and no space group was identified. In the first study, Sr_2ScSbO_6 was reported as orthorhombic with unit cell parameters a=5.678 Å; b=5.691 Å; c=8.021 Å [17]. The second work reported Sr_2ScSbO_6 as tetragonal, with a=8.019 Å; c=8.063 Å [7]. Also, there are no previous studies on the possible temperature driven phase transitions in both materials. The aim of this work is also to analyze the possible high-temperature phase-transitions in these compounds.

2. Experimental

2.1. Sample preparation

Polycrystalline samples of A_2ScSbO_6 (A=Sr,Ca) were prepared by the conventional solid state reaction method with acetone, as described previously [12–14]. Stoichiometric amounts of the reacting compounds were mixed according to the following chemical reaction:

$$4ACO_3 + Sc_2O_3 + Sb_2O_5 \longrightarrow 4A_2ScSbO_6 + 2CO_2 (A = Ca,Sr).$$

The reacting compounds (all delivered by Sigma-Aldrich) had the following purities: $SrCO_3$ (99.995+%) or $CaCO_3$ (99.999%), Sc_2O_3 (99.995%) and Sb_2O_5 (99.995%). All compounds were used as received. The starting materials were mixed and ground in an agate mortar with acetone and, subsequently, heated in air, in alumina crucibles. The following heat treatment was used: 12 h at 870 K, 12 h at 1270 K, 24 h at 1470 K and 72 h at 1770 K, with cooling and regrinding after

* Corresponding author at: CICenergigune, Parque Tecnológico, Albert Einstein 48, 01510 Miñano, Álava, Spain. Fax: +34 945297108.
E-mail address: afaik@cicenergigune.com (A. Faik).

0022-4596/$ - see front matter © 2012 Elsevier Inc. All rights reserved.
http://dx.doi.org/10.1016/j.jssc.2012.04.019

each heating. To control the quality of the obtained material, X-ray diffraction measurements were performed after each heating. Pure phases were obtained for both compounds.

2.2. Diffraction measurements and data analysis

High-quality room-temperature diffraction data were obtained on a Bruker D8 Advance diffractometer equipped with a primary germanium para-focusing monochromator and Bragg-Brentano geometry, using Cu$K\alpha1 = 1.5406$ (Å) radiation. A Sol-X energy dispersive detector was used, with a detection window optimized for Cu$K\alpha1$, to avoid the fluorescence radiation from the samples. The data were collected between 15 and 110° in 2θ, with steps of 0.01° (2θ) and a counting time of 10 s per step.

High-temperature X-ray powder diffraction data were recorded on a similar Bruker D8 Advance diffractometer, equipped with a Våntec high speed one dimensional detector, using Cu$K\alpha$ radiation. An Anton Paar HTK2000 high-temperature chamber with direct sample heating (Pt filament) and a temperature stability of 0.5 K was used. The specimens for high-temperature measurements were prepared by mixing the material under study with acetone. Then, the mixture was 'painted' over the Pt-strip heater of the chamber. The high-temperature diffraction experiments were performed for Sr_2ScSbO_6 and Ca_2ScSbO_6 materials. To establish the presence of phase transitions and their temperatures, X-ray data were collected in narrow 2θ region, with a 5 K temperature step, using a continuous scan, with steps of 0.0167° (2θ), and a counting time of 12 s per step. Then, in order to obtain reliable values for the temperature evolution of the cell parameters, X-ray data were collected in the 15 to 120° (2θ) interval, with a 10 K temperature step between 300 K and 710 K for Sr_2ScSbO_6 and between 870 K and 1470 K for Ca_2ScSbO_6. Special attention was paid to the additional peaks belonging to the Pt sample heater that are present in the high-temperature diffractograms, and that overlap with the peaks originating from the samples. These peaks were excluded from the refinement.

Neutron powder diffraction (NPD) patterns were collected using the multi-counter fine-resolution powder diffractometer E9 installed at the Berliner Neutron Scattering Center (BENSC), at the Hahn-Meitner-Institute. The E9 diffractometer is equipped with a detector bank that covers 160°. However, it consists of individual ^{3}He tubes, each able to detect neutrons only at a particular place within a range of 2.5° with a resolution of about 10 min. The incident-neutron wavelength was 1.79776 Å. A high-temperature furnace was used between 300 and 1200 K. For these measurements, the powder sample of Sr_2ScSbO_6 was placed in a cylindrical vanadium container (outside: 8 mm, length: 47 mm). The data were collected in the range $10° < 2\theta < 160°$ with a non-linear step width of about 0.1°, during 8 h for each temperature.

The Rietveld refinement of the structures was performed using the WinPlotr/FullProf package [18]. The peak shape was described by a pseudo-Voigt function in the case of X-ray data and by a pseudo-Voigt function convoluted with axial divergence asymmetry function in the case of neutron data; the background level was modeled using a polynomial function. The refined parameters were: scale factor, zero shift, lattice constants, peak profile, asymmetry parameters, atomic positions or the amplitudes of the symmetry-adapted modes, and independent isotropic atomic displacement parameters. In the case of the neutron data the resolution function provided at the instrument was used.

3. Results and discussion

3.1. Room-temperature crystal structures of Sr_2ScSbO_6 and Ca_2ScSbO_6

The ideal double perovskite with the general formula $A_2BB'O_6$ has a cubic symmetry with the space group $Fm\overline{3}m$. This symmetry is usually expected when the tolerance factor values t is close to unity ($t = (r_A + r_O)/\sqrt{2}(\overline{r}_{B,Sb} + r_O)$ where $\overline{r}_{B,Sb}$ is the averaged ionic radius of the B and B' cations). For the majority of double perovskites, however, the size of the A-cation is too small to fit in the cavity formed by the 12 anions. In such cases, tilting of the octahedra generally occurs, leading to a lower symmetry and, hence, for the structure distorted from prototype cubic symmetry, the value of t is < 1. The tolerance factors, at room temperature for Sr_2ScSbO_6 and Ca_2ScSbO_6 are 0.969 and 0.897, respectively (calculated using the ionic radii given in [19]). These values suggest that the room-temperature structures of both compounds should not be cubic and the calcium compound will be more distorted than the strontium one.

The room-temperature data obtained for Sr_2ScSbO_6 from neutron powder diffraction (NPD) and X-ray powder diffraction (XRPD) measurements, refined simultaneously to determine the structure, are shown in Fig. 1a and b, respectively. The refinement process has been done using the new version (July 2011) of FullProf Suite program [18]: making use of symmetry-adapted modes as it will be explained below.

In Fig. 1a and b, many diffraction lines are clearly split, indicating that the unit cell of this material is not cubic as expected. The insets in Fig. 1a and b show the splitting of the (800) cubic reflection. As a starting model for the Rietveld refinement, we have used the lowest symmetry space group usually encountered in the case of the ordered antimony double perovskite oxides: the monoclinic structure with space group $P2_1/n$ suggested in [13], with the following atomic positions: Sb at $2c$ (0, 1/2, 0), Sc at $2b$ (1/2, 0,0) and Sr, O_1, O_2 and O_3 at $4e$ (x,y,z). The structural details of Sr_2ScSbO_6 at room temperature are given in Table 1. A large number of weak reflections are observed in both diffraction patterns. The enlarged portion of the profile shows the presence of the primitive (monoclinic) Bragg peaks (111/−111) at about 24.75 in XRPD data, (210/120) at 41.38° and (−212/212/−122/122) at 49.44° in NPD data, that violate the I-centering condition on the hkl reflections with $h+k+l = 2n$.

For the Ca_2ScSbO_6, the Rietveld refinement results of X-ray diffraction pattern data recorded at room temperature are shown in Fig. 2. All diffraction lines are indexed based on a monoclinic symmetry with the $P2_1/n$ space group, the unit-cell being: $a = 5.5088(1)$ Å; $b = 5.6226(1)$ Å; $c = 7.8601(1)$ Å and $\beta = 90.02(1)°$. A clear splitting of many peaks can be observed, inset of Fig. 2. The final atomic parameters, cell parameters and isotropic atomic displacement parameters are listed in Table 1.

The monoclinic structure ($P2_1/n$ space group) of the double perovskite oxide with general formula $A_2BB'O_6$ is characterized by rock-salt like ordering, of the Sc^{3+} and Sb^{5+} cations, over alternative layers. The degree of cation ordering depends mostly on the charge difference, size, and polarization of B- and B'-site cations. The Sc and Sb atoms are totally ordered in the two distinct B sites, in both compounds Sr_2ScSbO_6 and Ca_2ScSbO_6, due to the significantly larger difference in the effective ionic radii of the Sc^{3+}–Sb^{5+} ($\Delta r = 0.145$ Å).

Table 2 lists the main interatomic distances and the angles for Sr_2ScSbO_6 and Ca_2ScSbO_6 phases at room temperature. The structural analysis of both compounds indicates that the Sc^{3+} and Sb^{5+} are octahedrally coordinated with the oxygen atoms. The typical Sc–O bond lengths of ScO_6 octahedra range between 2.04 and 2.10 Å. Similarly, the Sb–O bond lengths of SbO_6 octahedra range between 1.96 and 2.01 Å. The average $\langle Sc-O \rangle$ and $\langle Sb-O \rangle$ are also close to the calculated values from the ionic radii: 2.15 Å and 2.00 Å, respectively. The ScO_6 and SbO_6 octahedra are alternatively connected and extended in three dimensions. The A^{2+} cations are located in the cavities formed by the corner-sharing octahedra, the average of the A–O short distances 2.85 Å is typical for Sr^{2+} cations in a 12-coordinate environment and 2.62 Å for Ca^{2+} in a 9-coordinate environment. This is commonly observed for compositions that

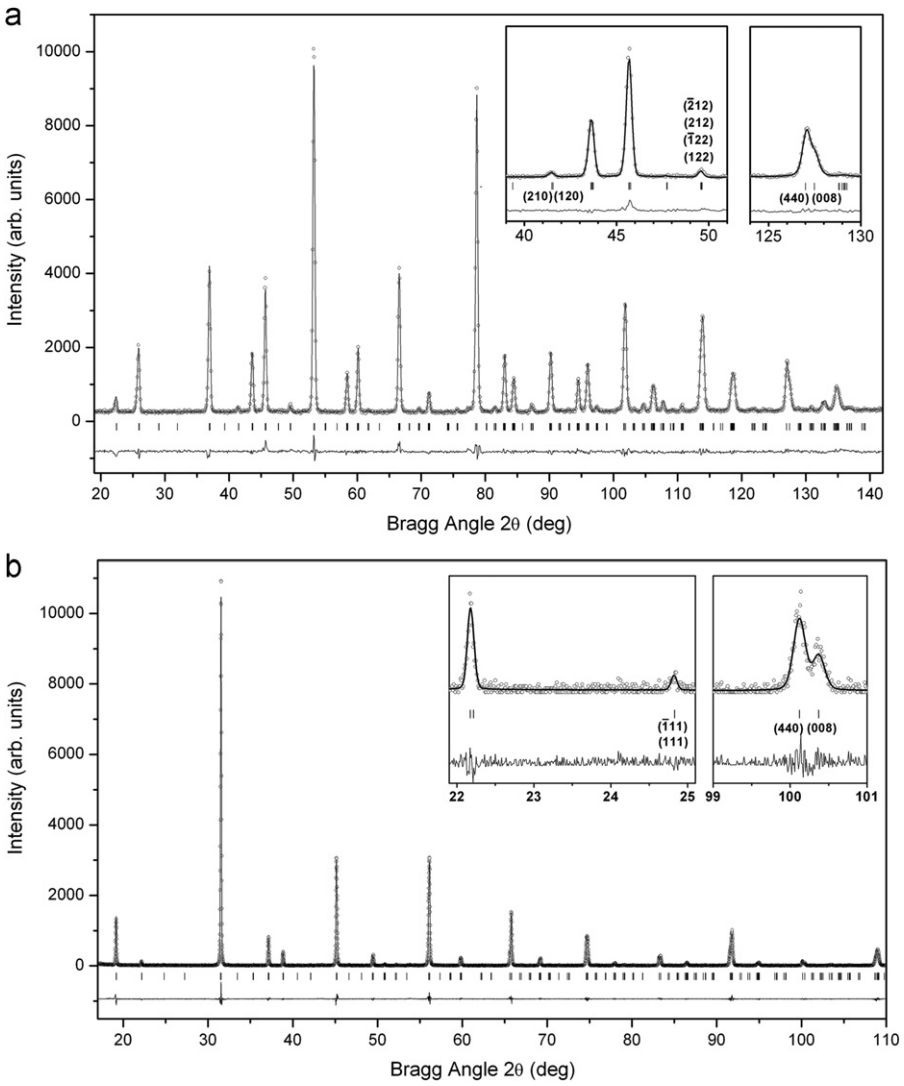

Fig. 1. Experimental (symbols) and calculated (line) neutron profiles (top) and X-ray profiles (bottom) for the Rietveld refinement of Sr_2ScSbO_6 at room temperature using a structural model with $P2_1/n$ space group. Insets show in detail the presence of the primitive Bragg peaks corresponding to the $P2_1/n$ symmetry.

Table 1
Crystal structure and Reliability factors for Sr_2ScSbO_6 and Ca_2ScSbO_6, the atomic positions were refined in space group $P2_1/n$ at room temperature from X-ray and E9 neutron data.

Compound R. factors	Lattice parameters	Atom (site)	x	y	z	B(Å^2)	Occupancy
Sr_2ScSbO_6 (X-ray/Neutron)		Sr(4*e*)	0.0021(2)	0.0099(3)	0.2487(5)	0.50(3)	1.00
$R_p = 9.80/5.24\%$	$a=5.6915(1)$ Å	Sb(2*c*)	0	1/2	0	0.28(3)	1.00
$R_{wp} = 17.0/6.84\%$	$b=5.6778(1)$ Å	Sc(2*d*)	1/2	0	0	0.31(5)	1.00
$\chi^2 = 1.66/2.53$	$c=8.0244(1)$ Å	O_1(4*e*)	0.2615(2)	0.2680(2)	0.0280(4)	0.30(3)	1.00
$R_{Bragg} = 4.29/3.85$	$\beta=90.03(1)^\circ$	O_2(4*e*)	0.2740(2)	0.2620(2)	0.4770(2)	0.60(4)	1.00
	$V=259.31(1)$ Å^3	O_3(4*e*)	0.9493(2)	0.4944(2)	0.2456(2)	1.00(2)	1.00
Ca_2ScSbO_6 (X-ray)		Ca(4*e*)	0.0150(9)	0.0461(4)	0.2490(4)	0.28(6)	1.00
$R_p = 10.9\%$	$a=5.5088(1)$ Å	Sb(2*c*)	0	1/2	0	0.18(3)	1.00
$R_{wp} = 16.0\%$	$b=5.6226(1)$ Å	Sc(2*d*)	1/2	0	0	0.59(6)	1.00
$\chi^2 = 3.11$	$c=7.8601(1)$ Å	O_1(4*e*)	0.292(2)	0.303(2)	0.052(2)	0.48(3)	1.00
$R_{Bragg} = 3.55$	$\beta=90.02(1)^\circ$	O_2(4*e*)	0.299(2)	0.284(2)	0.444(2)	0.48(3)	1.00
	$V=243.46(1)$ Å^3	O_3(4*e*)	0.908(2)	0.468(1)	0.244(1)	0.48(3)	1.00

include an A^{2+} cation which is too small to fill the twelvefold coordination site, and results in a reduced nine-fold coordination environment for the A cation in the monoclinic structure. The mean average distance A–O decreases as Sr^{2+} is substituted by Ca^{2+}, which is consistent with the lower ionic radius of Ca^{2+}(1.23 Å) compared to Sr^{2+}(1.44 Å). This smaller size of Ca^{2+} is responsible for the larger monoclinic distortion. The tilt of the octahedra is inferred from the deviation of Sc–O–Sb angles from the ideal value (180°), the

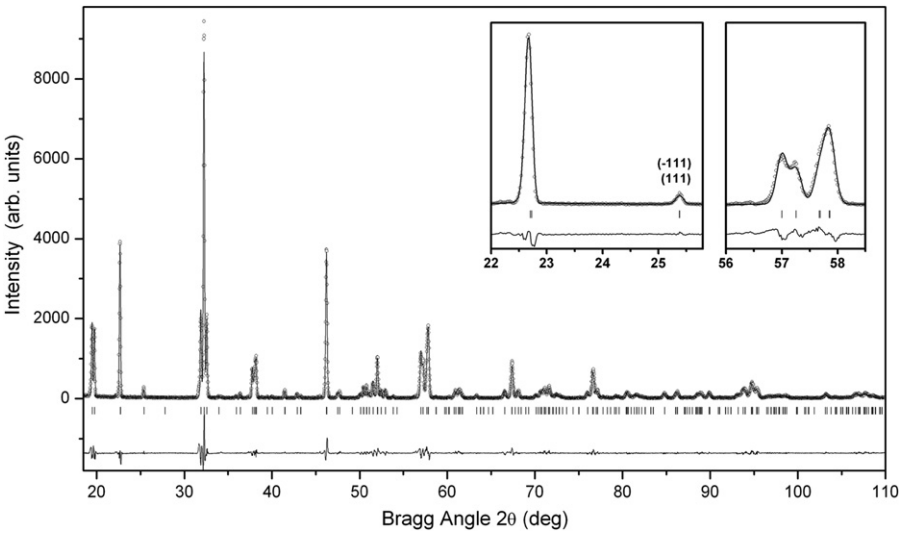

Fig. 2. Experimental (symbols) and calculated (line) X-ray powder diffraction profiles for the Rietveld refinement of Ca_2ScSbO_6 at room temperature using a structural model with $P2_1/n$ space group. Insets show in detail the presence of the primitive Bragg peaks corresponding to the $P2_1/n$ symmetry.

Table 2
Main bond distances (Å), selected angles (deg) and octahedra tilt angles (deg) for Sr_2ScSbO_6 and Ca_2ScSbO_6 from XRPD at room temperature. $rSc^{3+}(VI) = 0.745$ Å $rSb^{5+}(VI) = 0.6$ Å.

	Sr_2ScSbO_6	Ca_2ScSbO_6
ScO_6 polyhedra		
Tilt angle $\psi_{[001]p}$	4.28(2)	9.20(2)
Tilt angle $\phi_{[110]p}$	7.72(9)	15.0(2)
Sc-O_1 (× 2)	2.052(2)	2.091(9)
Sc-O_2 (× 2)	2.072(2)	2.092(9)
Sc-O_2 (× 2)	2.062(2)	2.078(9)
Average distance	2.062(4)	2.087(4)
Predicted distance	2.145	2.145
SbO_6 polyhedra		
Tilt angle $\psi_{[001]p}$	3.82(2)	11.0(3)
Tilt angle $\phi_{[110]p}$	8.19(9)	15.7(2)
Sb-O_1 (× 2)	2.001(2)	1.997(9)
Sb-O_2 (× 2)	1.975(2)	1.992(9)
Sb-O_3 (× 2)	1.992(2)	1.995(9)
Average distance	1.989(4)	1.995(4)
Predicted distance	2.000	2.000
AO_n polyhedra		
A-O_1 (× 1)	2.733(4)	2.610(2)
A-O_1 (× 1)	2.628(4)	2.333(3)
A-O_1 (× 1)	3.109(5)	–
A-O_1 (× 1)	2.914(5)	2.811(5)
A-O_2 (× 1)	2.792(3)	2.564(2)
A-O_2 (× 1)	2.625(4)	2.352(2)
A-O_2 (× 1)	3.115(5)	–
A-O_2 (× 1)	2.848(5)	2.842(5)
A-O_3 (× 1)	2.942(9)	–
A-O_3 (× 1)	2.767(9)	2.447(7)
A-O_3 (× 1)	2.571(2)	2.372(9)
A-O_3 (× 1)	3.124(2)	3.207(9)
Average distance	2.847(4)	2.615(6)
Predicted distance	2.84	2.63
Sb-O_1-Sc (× 2)	165.6(4)	148.6(3)
Sb-O_2-Sc (× 2)	166.7(5)	149.0(4)
Sb-O_3-Sc (× 2)	163.5(6)	149.5(4)
⟨Sb−O−Sc⟩	165.3	149.0

deviation is bigger in the case of Ca compound (the average angle is 149°) in comparison to the Sr compound (the average angle is 165°).

Glazer proposed a simple notation for clarifying and describing the possible space groups of simple perovskites by allowing for octahedral tilting [20]. Woodward extended it to describe the double perovskites with the general formula $A_2BB'O_6$ [21]. Using this notation, a tilt system is described in terms of rotations of BO_6 octahedra around any of the cartesian axes. These axes are coincident with the three axes of the prototype unit cell of the cubic simple perovskite ($Pm\bar{3}m$ space group). When the unit cell of primitive perovskites ABO_3 is described as $a_p \times a_p \times a_p$, that of the double-type perovskites should be described as $2a_p \times 2a_p \times 2a_p$ (cubic) or $\sqrt{2}a_p \times \sqrt{2}a_p \times 2a_p$ (tetragonal or monoclinic). The relative orientation of the unit cell of the prototype cubic ($Pm\bar{3}m$) of simple perovskite and those of the prototype cubic ($Fm\bar{3}m$), tetragonal ($I4/m$) and monoclinic ($I2/m$ and $P2_1/n$) of the double perovskites are shown in Fig. 3. On the other hand, in Fig. 4 we show the projections, along the cubic (simple) perovskite axes, ($[100]_p$, $[010]_p$ and $[001]_p$), of the structure of the double perovskite with $A_2BB'O_6$ general formula in the $Fm\bar{3}m$, $I4/m$, $I2/m$ and $P2_1/n$ space groups, to show that the difference amongst the structural models consists in the losing of one or more tilts around the simple perovskite axis.

A group–subgroup relation necessarily exists between the space groups of the prototype structure and the observed distorted one. The structural distortion that relates them can be identified as a symmetry breaking distortion. Usually small distortions (only for displacive type, in our case) imply that the parent phase can be thermally stabilized, and one or several structural phase transitions toward the arrangement of higher symmetry may happen as temperature increases. The distortion presents in a distorted structure can be studied by means of the symmetry-mode analysis. This distortion usually contains a primary component, corresponding to a symmetry mode or modes which are unstable in the parent high-symmetry configuration, and are fundamental for explaining the stability of the distorted structure. In addition, the distortion contains other secondary contributions of less importance, associated with modes which are allowed by symmetry and become frozen through coupling with the primary ones. Those distortion modes are associated with different irreducible representations (irreps) of the parent space group. The symmetry-mode analysis consists on the separation of the different modes contributions in a structural distortion.

The program AMPLIMODES [22] performs the symmetry-mode analysis for a given distortion between a prototype and a distorted structure. There is also a module available that prepares a special input file (pcr-file) suitable for refining powder-diffraction data using the FullProf Package. Using this pcr-file FullProf will refine the amplitudes of the symmetry modes instead of the usual atomic

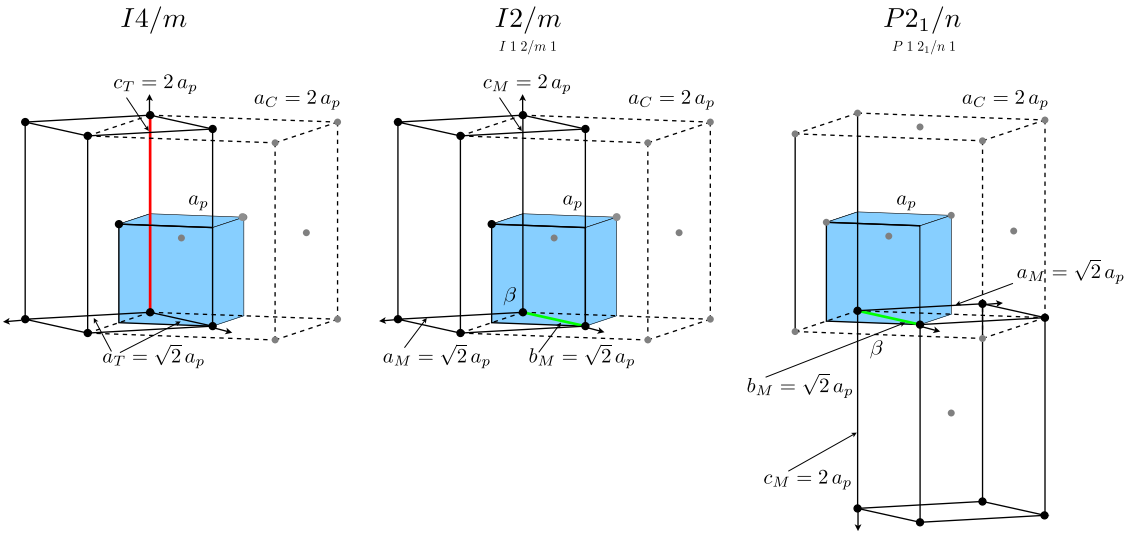

Fig. 3. The relative orientation of the unit cell of the prototype cubic simple perovskite ($Pm\bar{3}m$) (blue) and those of the prototype cubic ($Fm\bar{3}m$) (dashed lines, the distorted tetragonal ($I4/m$) and the monoclinic ($I2/m$ and $P2_1/n$) of the double perovskites. (For interpretation of the references to color in this figure caption, the reader is referred to the web version of this article.)

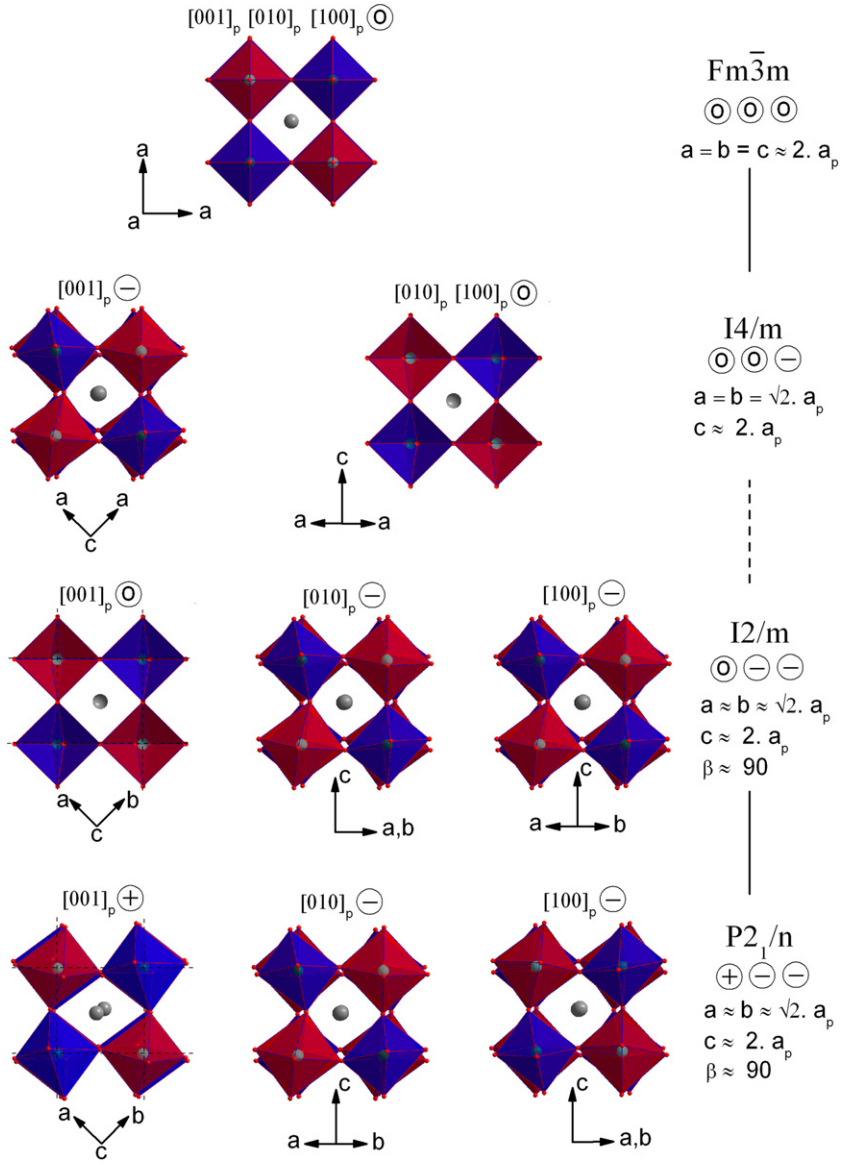

Fig. 4. Projections along the cubic (simple) perovskite axes, ($[100]_p$, $[010]_p$ and $[001]_p$), of an unit cell section of the structure of Sr_2ScSbO_6 in the $Fm\bar{3}m$, $I4/m$, $I2/m$ and $P2_1/n$ space groups showing in-phase (+), out-of-phase (−) rotations. ScO_6 octahedra are shown in red, SbO_6 in blue and Sr atoms in grey. Each structural transition corresponds to the appearance or/and the disappearance of these rotations. (For interpretation of the references to color in this figure caption, the reader is referred to the web version of this article.)

coordinates. It is expected that this new basis will be better adapted to describe the distortion and, thus, will simplify the process of the refinement [23]. Very recently, this approach, the module of AMPLIMODES and the new version of FullProf have been proven to be very efficient and very robust for refining powder diffraction data [24].

Given the parent ($Fm\bar{3}m$ space group) and the distorted structure (the room-temperature monoclinic symmetry, $P2_1/n$ space group), AMPLIMODES calculates the atomic displacements relating both structures, if their magnitudes lay within some tolerance range. A complete basis of symmetry-adapted distortion modes is then determined and defined. Then, the program decomposes the distortion in terms of this basis of symmetry modes, and calculates the amplitudes for each of the symmetry-adapted distortions. Modes are given in terms of atomic displacements in relative units for the atoms of the asymmetric unit of the distorted phase. It is worth noting that for the symmetry-mode analysis in AMPLIMODES it is not necessary to know a real parent structure. The contributions of the much more important symmetry-breaking distortion-modes present in the distorted phase do not depend on any choice of the atomic coordinates of the parent structure.

Table 3
Summary of the mode decomposition of $P2_1/n$, $I2/m$ and $I4/m$ with respect to their $Fm\bar{3}m$ parent structure of Sr_2ScSbO_6.

Space group	Irrep	K-vector	Direction	Isotropy subgroup	Dimension	Amplitude (Å)
$P2_1/n$	GM^{1+}	(0,0,0)	(a)	$Fm\bar{3}m$	1	0.203(9)
	GM^{3+}	(0,0,0)	(a,0)	$I4/mmm$	1	0.06(1)
	GM^{4+}	(0,0,0)	(a,a,0)	$C2/m$	1	0.80(1)
	GM^{5+}	(0,0,0)	($-b$,a,$-a$)	$C2/m$	4	0.049(7)
	X^{2+}	(0,1,0)	(0,a,0)	$P4_2/mnm$	1	0.019(5)
	X^{3+}	(0,1,0)	(0,a,0)	$P4/mnc$	1	0.404(5)
	X^{5+}	(0,1,0)	(a,a,0,0,a,$-a$)	$Pnnm$	3	0.132(3)
$I2/m$	GM^{1+}	(0,0,0)	(a)	$Fm\bar{3}m$	1	0.205(8)
	GM^{3+}	(0,0,0)	(a,0)	$I4/mmm$	1	0.001(9)
	GM^{4+}	(0,0,0)	(a,a,0)	$C2/m$	1	0.54(1)
	GM^{5+}	(0,0,0)	($-b$,a,$-a$)	$C2/m$	4	0.015(9)
$I4/m$	GM^{1+}	(0,0,0)	(a)	$Fm\bar{3}m$	1	0.203(6)
	GM^{3+}	(0,0,0)	(a,0)	$I4/mmm$	1	0.001(8)
	GM^{4+}	(0,0,0)	(0,0,a)	$I4/m$	4	0.500(2)

In Table 3 we show the results of the mode analysis carried out by AMPLIMODES for the different phases of Sr_2ScSbO_6. The reference structure is the prototype cubic, determined from the high-temperature XRPD data, and the "low-symmetry" phases are NPD-data structures obtained at different temperatures (Fig. 5a).

In the case of Sr_2ScSbO_6 and Ca_2ScSbO_6, there are six irreps of the $Fm\bar{3}m$ space group (the seventh irrep, GM^{1+}, is the totally symmetric) that can take part in the symmetry breaking from that space group to the room-temperature $P2_1/n$ monoclinic space group: $GM^{3+}(1)$, $GM^{4+}(1)$, $GM^{5+}(4)$, $X^{2+}(1)$, $X^{3+}(1)$ and $X^{5+}(3)$. The numbers in parenthesis indicate the number of modes transforming according to the irreps, there are 11 modes (+1 totally symmetric). The 12 modes move the oxygen atoms (24e) (8 (+1) modes) and the A atoms (Sr or Ca) (8c) (3 modes). The atomic displacements defined by a mode imply a break of the symmetry of the prototype structure to the isotropy group symmetry, which is intermediate in the group–subgroup relation between the space groups of the reference and the distorted structures. Considering the graph of maximal subgroups shown in Fig. 5a it is clear that a combination of at least two primary modes of different symmetries is necessary to explain the whole symmetry break, one mode with symmetry X^{2+}, X^{3+} or X^{5+} together with a mode with symmetry GM^{4+} or GM^{5+}. The final result of the refinement is indicated as the value of the amplitude associated to each mode (this is the output of the FullProf program, as indicated in Table 3) or as the global amplitude value associated to each irrep. A representation of the polarization vectors of the different modes are shown in Fig. 6.

In the case of Sr_2ScSbO_6, looking at the refinement final-values for the amplitudes, it is clear that there are only two amplitudes considerable higher than the rest: 0.80(1) (GM^{4+}) and 0.404(5) (X^{3+}), if we exclude the totally symmetric one, i.e. 0.203(9) (GM^{1+}). The symmetry of the intermediate phase $I2/m$ is compatible with the fact that the mode GM^{4+} shows a larger amplitude, i.e. it is more unstable in the parent configuration and is the first to freeze. The other amplitudes are negligible, their associated sigma's indicate that they can be "rounded" to zero. There are two primary modes that must be coupled and give rise to the observed room-temperature broken symmetry. This coupling of the unidimensional GM^{4+} and X^{3+} modes is shown in Fig. 7a. It is worth mentioning that the coupled primary modes only involve oxygen atoms, and comparing the new configuration resulting from the coupling of the unidimensional GM^{4+} and X^{3+} modes with the $a^+b^-b^-$ tilting scheme associated to $P2_1/n$: the atomic displacements implied by the two coupled primary modes can be interpreted,

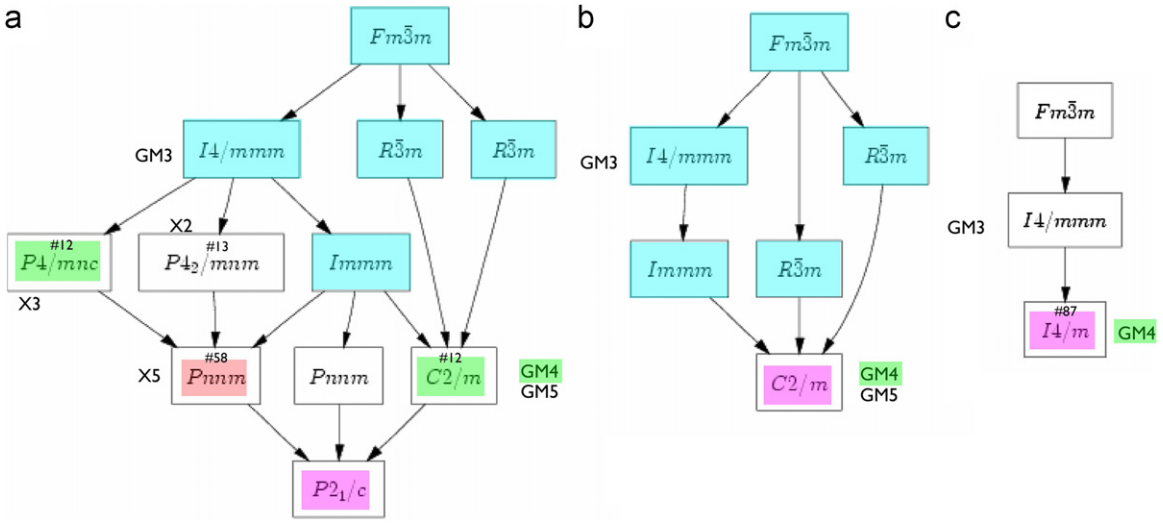

Fig. 5. Graph of maximal subgroups relating the space groups of the parent and distorted phases of Sr_2ScSbO_6.

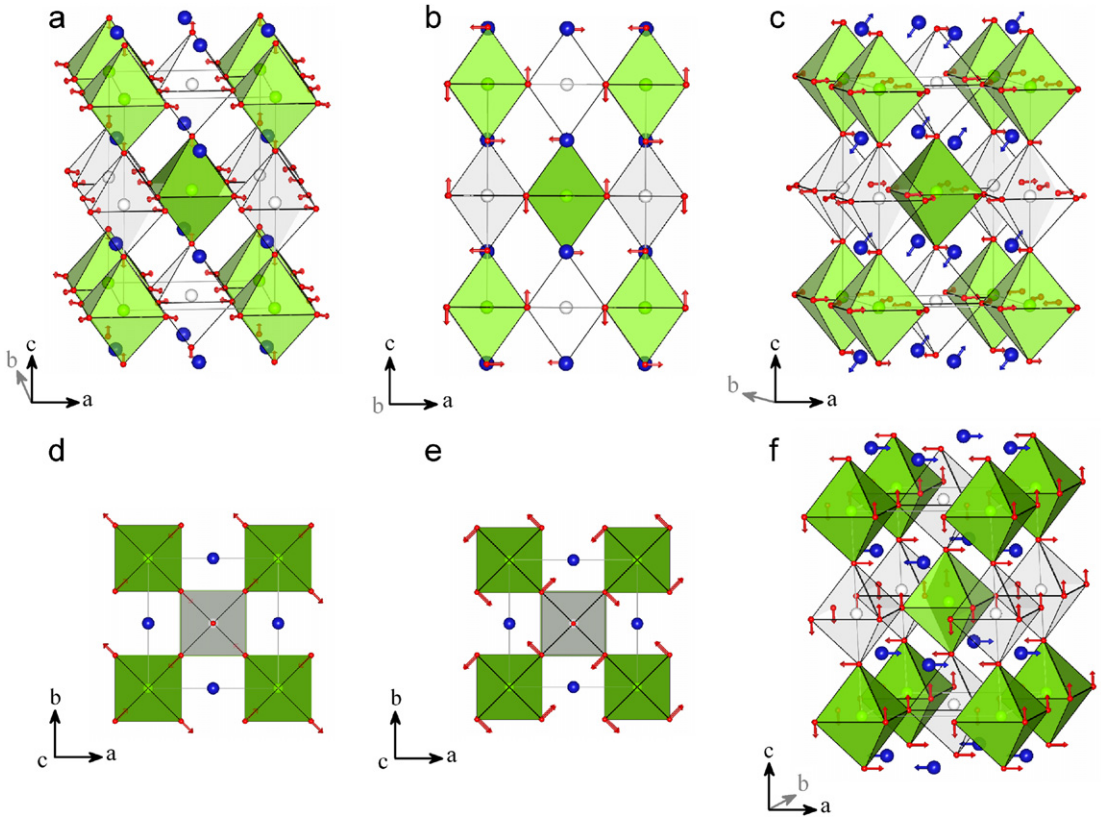

Fig. 6. Scheme of the polarization vectors of the six different irrep distortion components of the $Fm\bar{3}m$ space group that can take part in the symmetry breaking from that space group to the room-temperature $P2_1/n$ monoclinic space group: GM^{3+}(a), GM^{4+}(b), GM^{5+}(c), X^{2+}(d), X^{3+}(e) and X^{5+}(f).

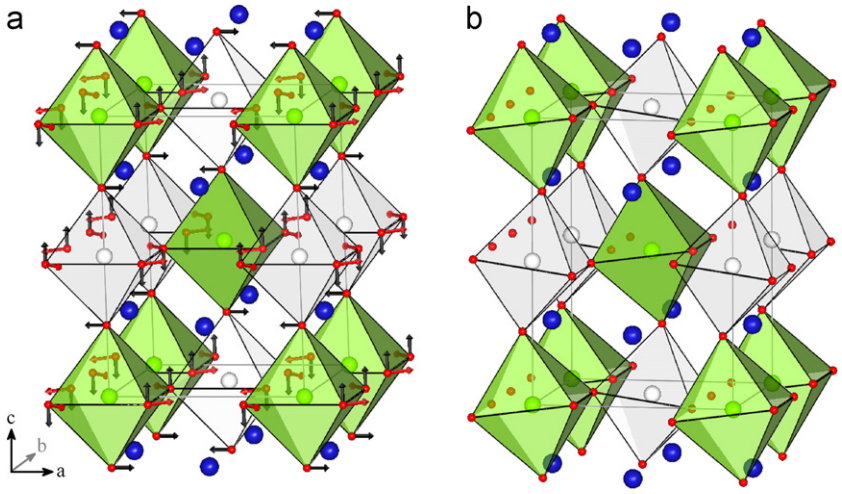

Fig. 7. Representation of the new configuration resulting from the coupling of the unidimensional GM^{4+} and X^{3+} modes with the $a^+b^-b^-$ tilting scheme associated to $P2_1/n$: the atomic displacements implied by the two coupled primary modes can be interpreted, precisely, as the rotations (tilts) of the octahedra.

precisely, as the rotations (tilts) of the octahedra (Fig. 7b). Hence, the physically more sensitive (making full use of symmetry consideration restrictions) refinement procedure gives rise directly and naturally (the amplitudes of the non-primary modes round to zero) to the physically observed distortions.

Although it was not refined using the symmetry modes, the symmetry-mode analysis can also be applied to the room temperature phase of Ca_2ScSbO_6. The results are resumed in Table 4. For this compound, again, the main amplitudes correspond to modes with irreps GM^{4+} and X^{3+} (1.57(5) Å and 0.99(4) Å, respectively) which would suggest a similar path for the different phase transitions of this compound (three phase transitions were found for Sr_2ScSbO_6 at 400, 560 and 650 K). As it will be explained later, only the first of these transitions (from $P2_1/n$ to $I2/m$ at about 1440 K) was observed in our experiments. The absence of the other two phase transitions and the high temperature at which the observed one happens (compared to the temperature corresponding to the first phase transition of Sr_2ScSbO_6) can be explained by the fact the primary modes show a larger amplitude and that another mode, X^{5+} is also relevant in this structure. This mode is the responsible of the displacement of the *A*-type atom along the monoclinic axis, a displacement that is 5 times larger in the case of Ca than in the case of Sr.

3.2. High-temperature X-ray and neutron diffraction of Sr_2ScSbO_6 and Ca_2ScSbO_6

In order to search the phase transitions in Sr_2ScSbO_6 at high temperatures, we analyzed two narrow 2θ intervals: 51.4° to 52.4° and 98° to 101° in the temperature range from 300 to 780 K, with a step of 5 K. The first one corresponding to the monoclinic primitive Bragg peaks (131/−131/311/−311) and the second one corresponding to the (642) cubic reflection, that has been identified as specially sensitive to the structural changes occurring in these kind of materials. Fig. 8 shows the evolution of diffraction intensities of these reflections with temperature. As shown in Fig. 8c, the primitive Bragg peaks disappear at about 400 K which no longer satisfy the $h+k+l=2n$ reflection condition. This corresponds to a transition from the primitive space group $P2_1/n$ to a centered space group. It is worth noting that the monoclinic splitting observed at room temperature is maintained up to 560 K, as we can see in Fig. 8a and b. These two facts are compatible with a continuous phase transition occurring at 400 K from the room-temperature $P2_1/n$ monoclinic space group to an I -centered monoclinic space group $I2/m$. High-resolution neutron diffraction measurements were performed at 430 K to determine the structural changes. The pattern calculated using the $I2/m$ space group shows a good agreement with the experimental pattern (Fig. 9) and provides good agreement factors. In the inset of Fig. 9, we can see how all of the primitive Bragg peaks present at low temperatures are missing. In Figs. 8a and b, we observe the appearance of a shoulder on the low-angle side of

Table 4
Summary of the mode decomposition of $P2_1/n$ with respect to the $Fm\bar{3}m$ parent structure of Ca_2ScSbO_6.

Space group	Irrep	K-vector	Direction	Isotropy subgroup	Dimension	Amplitude (Å)
$P2_1/n$	GM^{1+}	(0,0,0)	(a)	$Fm\bar{3}m$	1	0.00(3)
	GM^{3+}	(0,0,0)	$(a,0)$	$I4/mmm$	1	0.01(3)
	GM^{4+}	(0,0,0)	$(a,a,0)$	$C2/m$	1	1.57(3)
	GM^{5+}	(0,0,0)	$(-b,a,-a)$	$C2/m$	4	0.23(2)
	X^{2+}	(0,1,0)	$(0,a,0)$	$P4_2/mnm$	1	0.00(3)
	X^{3+}	(0,1,0)	$(0,a,0)$	$P4/mnc$	1	0.99(3)
	X^{5+}	(0,1,0)	$(a,a,0,0,a,-a)$	$Pnnm$	3	0.633(8)

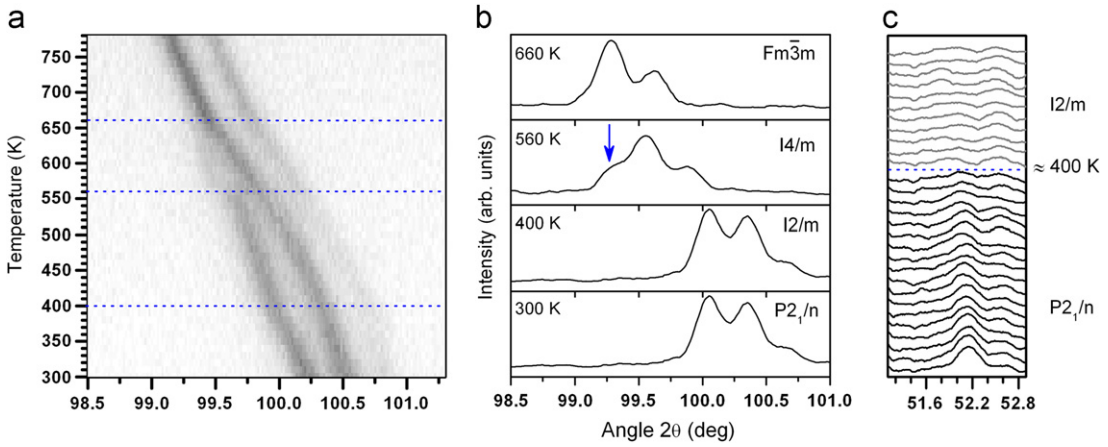

Fig. 8. Thermal evolution of XRPD of the (642) cubic reflections (a,b) and the primitive Bragg peaks (c) of Sr_2ScSbO_6. (a) scattered intensity is represented with shades of gray–black corresponds to high intensity, and white, to low intensity. (b) An arrow marked the shoulder appearing at 560 K. (c) Thermal evolution of the primitive Bragg peaks (131/−131/311/−311) showing disappears of these peaks at about 400 K.

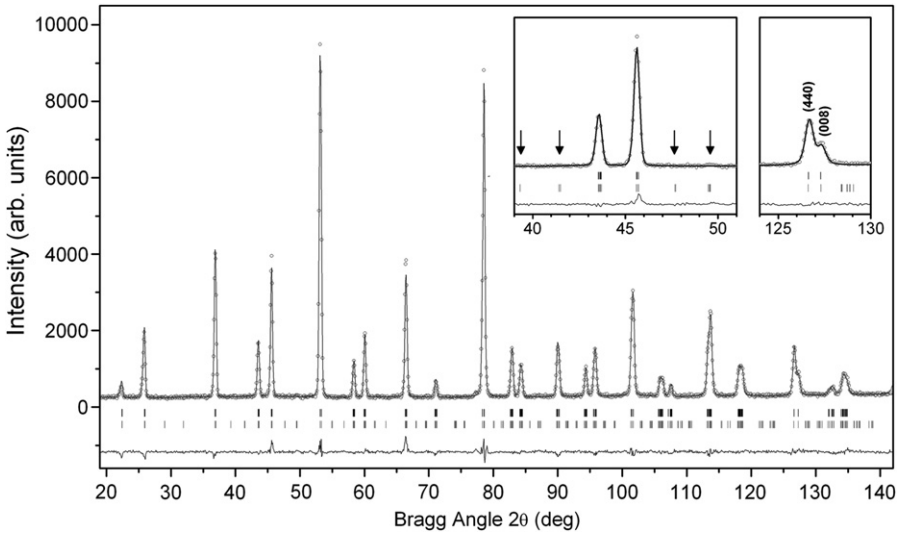

Fig. 9. Experimental (symbols) and calculated (line) neutron profiles for the Rietveld refinement of Sr_2ScSbO_6 at 430 K, using a structural model with $I2/m$ space group. The vertical bars indicate the Bragg reflections: those in the top row correspond to the $I2/m$ space group and the ones in the bottom row to $P2_1/n$ space group. Insets shows in detail the missing of the primitive Bragg peaks corresponding to the $P2_1/n$ symmetry.

the shown peak at 560 K. This is very similar to that observed in Sr_2CrSbO_6 [14], where this change was interpreted as an evidence of the material undergoing a discontinuous phase transition from a monoclinic structure to a tetragonal one with $I4/m$ space group. The refinement of NPD pattern at 633 K with $I4/m$ model gave a good fit of the diffraction profile and provided a good agreement factors as well. Structural details for Sr_2ScSbO_6 at 430 K in $I2/m$ and at 613 K in $I4/m$ are given in Table 5. The tetragonal distortion of the unit cell disappears in a continuous way and at about 660 K the unit cell transforms from tetragonal to cubic. It is the same transformation as that observed in other double perovskite materials presenting the $I4/m \rightarrow Fm\bar{3}m$ phase transition.

To determine the variation of the lattice constants with the temperature in Sr_2ScSbO_6 at high temperatures, we obtained 42 X-ray powder diffraction profiles, in 2θ range from 15° to 120°, at different temperatures between 300 K and 710 K, with a step of 10 K. The variation of unit cell parameters and space group symmetries of Sr_2ScSbO_6 with temperatures is shown in Fig. 10.

We have analyzed the temperature evolution structure in terms of modes of the two intermediate phases $I2/m$ and $I4/m$ present in Sr_2ScSbO_6, as deduced from the NPD data, using the AMPLIMODES program. The analysis is made in the same way as the experimental data are taken: starting from the low-temperature phase ($I2/m$ at 430 K) and increasing the temperature to end up in the cubic phase, following the convention in the Bilbao Crystallographic Server the monoclinic ($I2/m$) structure is described using the standard setting in $C2/m$. Although the phase-transition sequence is $I2/m \rightarrow I4/m \rightarrow Fm\bar{3}m$, both low-lying phases will have the same parent phase as the reference.

Nevertheless, due to experimental limitations related to the time-interval spent at each temperature at which data were collected, we did not reach the high-temperature cubic phase. In any case, as mentioned before in relation to the character of the parent phase, this fact does not limit at all the analysis, although, we will not be able to present a complete set of points ending at the high-temperature phase, even if the last measured temperature should correspond to the cubic phase. Also, there is a temperature difference between the temperature associated to the phase transition as deduced from the XRPD and NPD data ($T_{NPD} - T_{XRDP} = 30$). In a recent work [14], we also observed a similar shift between the phase-transition temperatures observed by XRPD and by NPD. This temperature difference can be due to the different heating techniques and the quantity of the samples used in the different measurements.

There are four irreps of the $Fm\bar{3}m$ space group (the fifth irrep, GM^{1+}, is the totally symmetric) that can take part in the symmetry break from that space group to the $I2/m$ monoclinic space group: $GM^{3+}(1)$, $GM^{4+}(1)$ and $GM^{5+}(4)$. It is worth noting that the output of SYMMODES [25] for the $Fm\bar{3}m$-to-$I2/m$ symmetry break is contained in the $Fm\bar{3}m$-to-$P2_1/n$ symmetry break, as indicated in Fig. 5b, so, as it was explained earlier on the analysis of the room-temperature phase of Sr_2ScSbO_6, it is expected for the GM^{4+} to be the primary mode on this phase as its isotropy group is the same as the observed space group (as it is the case for the GM^{5+} irrep) and it is the primary mode on a lower temperature phase. The final refinement results for the amplitude values of the modes involved in this symmetry break are shown in Table 3. These results confirm the expected behavior of the different modes, as only the amplitude of the mode with symmetry GM^{4+} has a significant value. The polarization vector associated with GM^{4+}, going down to $P2_1/n$ or going down just to $I2/m$ is the same, and it involves all the oxygen atoms in the monoclinic phases. GM^{4+} is essentially a rotation of the octahedra around the b axis in the monoclinic cell; although it also deforms a little bit the octahedra: the amount of rotation of the oxygens in the ab plane, ($\approx 0.25, \approx 0.25, \approx 0$) set of coordinates, and the one above and perpendicular to that plane, ($\approx 0, \approx 0, \approx 0.25$) set of coordinates, are not the same. In Fig. 6 the red arrows indicate the polarization vector of the transforming according to the GM^{4+} irrep.

We have refined NPD data at 430 K using the symmetry-adapted modes, AMPLIMODES for Fullprof [24]. The refined amplitudes of the modes corresponding to the four irreps are shown in Fig. 11. Amongst those irreps both, GM^{4+} and GM^{5+}, lower the cubic symmetry down to the monoclinic. But from their

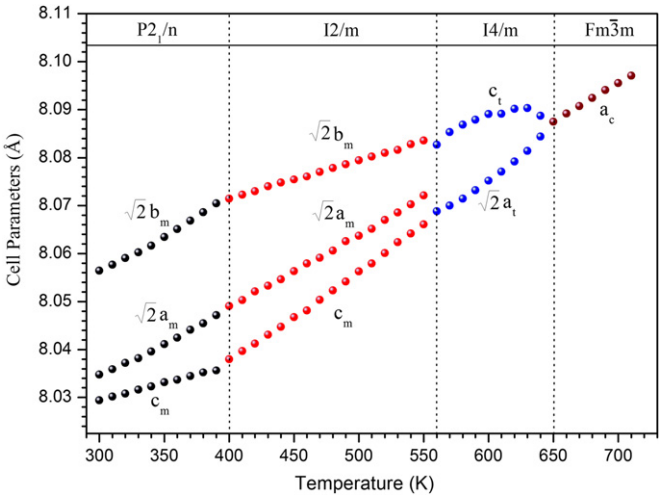

Fig. 10. Variation of the lattice parameters of Sr_2ScSbO_6 with the temperature. The high-temperature structure of this compound is cubic. Below 650 K it transforms to tetragonal. There is another phase transition at about 560 K, changing the symmetry from tetragonal to cantered monoclinic $I2/m$ and the last transition from centered monoclinic $I2/m$ to primitive monoclinic $P2_1/n$ at about 400 K.

Table 5
Crystal structure data and refinement results for Sr_2ScSbO_6 at 430 K and 613 K.

Temp. space group Agreement factors	Lattice parameters	Atom	Site	x	y	z	B(Å^2)
430 K ($I2/m$)	a=5.7021(1) Å	Sr	4*i*	0.4993(2)	0	0.2521(5)	0.69(3)
R_p = 4.84%	b=5.6861(1) Å	Sb	2*d*	0	0	1/2	0.44(1)
R_{wp} = 6.22%	c=8.0293(1) Å	Sc	2*a*	0	0	0	0.45(3)
χ^2 = 1.89	β=90.04(1)°	O_1	4*i*	−0.0484(8)	0	0.2439(9)	0.81(7)
R_{Bragg} = 3.18	V =260.33(1) Å^3	O_2	8*j*	0.2429(5)	0.2441(9)	0.0253(4)	0.90(6)
613 K ($I4/m$)	a=5.6929(1) Å	Sr	4d	0	1/2	1/4	1.04(4)
R_p = 5.65%	c=8.0641(1) Å	Sb	2a	0	0	1/2	0.51(4)
R_{wp} = 7.53%	V =261.35(1) Å^3	Sc	2*b*	0	0	0	0.79(7)
χ^2 = 2.83		O_1	4*e*	0	0	0.2455(5)	1.30(6)
R_{Bragg} = 4.54		O_2	8*h*	0.2770(4)	0.2125(4)	0	0.89(9)

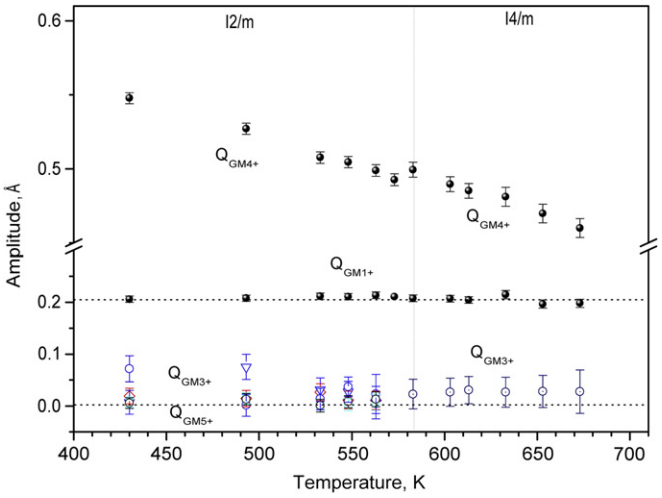

Fig. 11. The temperature evolution of the amplitudes of the GM^{1+}, GM^{3+}, GM^{4+} and GM^{5+} modes, as obtained from refinement of the NPD data of Sr_2ScSbO_6. The temperature at which the monoclinic structure disappears is 585 K.

amplitude values, it is clear that only GM^{4+} is responsible for the symmetry break, as its value is one order of magnitude bigger than the one corresponding to GM^{5+}. This mode involves only coordinates of the oxygens and the displacements shown in the mode pattern can be interpreted as tilts of the octahedra. The GM^{3+} symmetry mode is irrelevant for this phase transition, its amplitude values are two orders of magnitude lower than the primary mode one.

In the tetragonal ($I4/m$) to cubic ($Fm\bar{3}m$) phase transition there are two unidimensional modes (the third irrep, GM^{1+} is the totally symmetric), all of them involving oxygens atoms located at the (24*e*) *Wyckoff* positions of the prototype cubic phase: $GM^{3+}(1)$ and $GM^{4+}(1)$. The GM^{3+} mode is responsible for the breaking of the symmetry to the $I4/mmm$ tetragonal space group. This mode involves the movements of all the oxygen atoms in the octahedra, in a way that the oxygens located in the (00*z*) positions move to the center of the octahedra; and the oxygen atoms located in the *xy* plane move outwards along the diagonals of the basal plane of the octahedra. On the other hand, the mode GM^{4+} is responsible for the breaking of the symmetry down to the $I4/m$ space group, and involves movements only of the oxygens located in the *xy* plane. We have refined NPD data at 590 K using the symmetry-adapted modes. The result for the final amplitudes of the modes corresponding to the three irreps is shown in Table 3 and their evolution with the temperature is shown in Fig. 11. It can be readily appreciated that the GM^{4+} mode amplitude is considerable and shows a clear evolution with temperature. Their amplitude diminishes with the increasing temperature. The amplitude of the other mode (GM^{1+}) is negligible.

It is worth noting that despite the fact that the irreps of the primary modes lowering successively the symmetry from the cubic to the monoclinic ($I2/m$) are the same, in both cases involve only oxygen atoms, and in both cases, as well, can be interpreted as tilts of the octahedra, the cubic-to-tetragonal phase transition is continuous, and the tetragonal-to-monoclinic is discontinuous. The discontinuous character of the last transition is related to the change of the direction of the GM^{4+} irrep on the three-dimensional representation space as it can be seen in Table 3. The direction of the GM^{4+} irrep in the $I4/m$ phase is (0,0,*a*) while it changes to (*a*,*a*,0) in the monoclinic phases. From a structural point of view, this change of the direction is reflected on the relative orientation of both space groups: $I2/m$ is a subgroup of $I4/m$, but when the twofold axis is located in the same direction as the fourfold one, which is not the case. There is no way to go in a continuous manner from the tetragonal to the monoclinic symmetry when the twofold axis is perpendicular to the fourfold axis, as it is the case in the tetragonal-to-monoclinic phase transition, as shown in Fig. 3.

Another interesting remark is that the amplitudes of the primary modes and of the non-primary modes vary in the same temperature interval, as shown in Fig. 11, but the former show a trend in their variation, as expected, and the latter show a chaotic variation: no trend at all (some of them are very close to zero). The non-appreciable change in the amplitude value through the discontinuous $I2/m$ to $I4/m$ phase transition is not surprising. In fact, it is the same order parameter, with different symmetries, oriented in a different way. It is a coincidence that the labels for the irreps are the same. Although is not expected a linear behavior of the evolution with the temperature of the mode amplitude. On the other hand, it also seems that it is going to zero at a higher temperature. This non-zero value obtained is related to the same experimental issue referred to not reach the cubic phase. It is clear that there can be a temperature shift in the temperature values form one experiment to the other: from the X-ray data to the neutron data.

In order to determinate the presence of phase transitions and evolution of unit cell parameters with temperature in Ca_2ScSbO_6, X-ray data were collected in 2θ intervals, between 300 K and 1740 K, with a temperature step of 5 K. The first one between 24° and 26° corresponding to the primitive Bragg peaks reflections (111/−111) and the second one from 91° to 96° corresponding to the (642), as previously. Fig. 12 shows the evolution of diffraction intensities of these reflections with temperature. From the profile shape characteristic reflections at 2θ from 91 to 96 in (Fig. 12b), it was concluded that up to 1740 K Ca_2ScSbO_6 does not transform to the tetragonal lattice ($I4/m$ space group) like Sr_2ScSbO_6. This shows that there is no change in the monoclinic distortion in all this range of temperatures. Analyzing the peak splitting, it becomes clear that at 1740 K the unit cell is monoclinic. After examination of all diffractograms, we observed at about 1440 K the continuous disappearance of diffraction peaks corresponding to primitive Bragg reflections with indices (*hkl*) of the type $h+k+l=2n+1$ (Fig. 12a). This corresponds to a continuous phase transition from monoclinic $P2_1/n$ to monoclinic $I2/m$ at about 1440 K. The evolution with temperature from 720 to 1680 K of the refined lattice parameters for Ca_2ScSbO_6 is shown in Fig. 13. The lattice parameters increasing continuously with temperature and the difference between $\sqrt{2}a$, $\sqrt{2}b$ and c lattice parameters decreases. But no anomaly change is noted.

This behavior comes in good agreement with the symmetry-mode analysis performed for the room temperature structure of

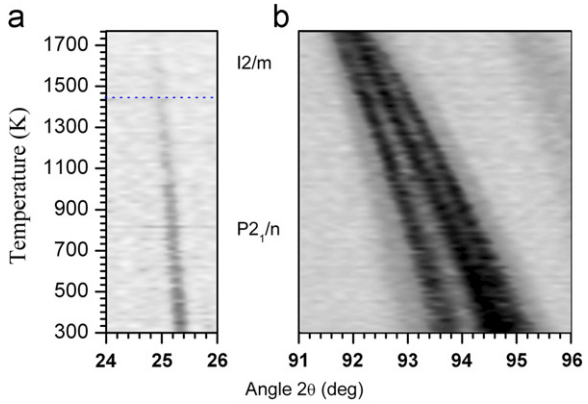

Fig. 12. Temperature evolution of the (642) cubic reflection of Ca_2ScSbO_6. In (b) scattered intensity is represented with shades of dark corresponds to high intensity and light to low intensity. The monoclinic splitting existing in the temperature range from 300 to 1700 K can be observed in (b). In (a) we observed dispersing of primitive Bragg peaks reflections at about 1440 K.

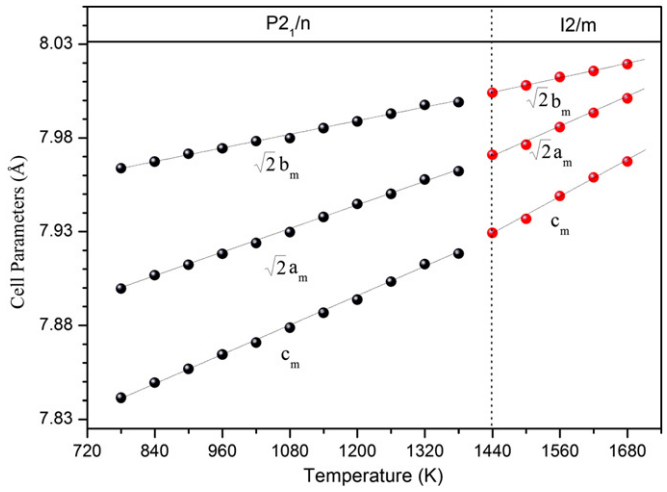

Fig. 13. Variation of the unit cell parameters of Ca_2ScSbO_6 with the temperature. There is a phase transition at about 1440 K changing the symmetry from the primitive monoclinic $P2_1/n$ to the centered monoclinic $I2/m$.

this compound. As it was explained earlier, the larger amplitudes of the primary modes together with the greater importance of the secondary ones imply a higher temperature for the stabilization of the tetragonal and cubic phases.

4. Conclusions

The objective of this investigation is to determine the crystal structures and phase transitions with temperature of the two ordered double perovskite oxides Sr_2ScSbO_6 and Ca_2ScSbO_6. The crystal structures at room temperature of both compounds are determined for the first time and are refined in monoclinic space group $P2_1/n$ with $a=5.6914(1)$ Å; $b=5.6776(1)$ Å; $c=8.0242(1)$ Å and $\beta=90.03(1)^\circ$ for Sr containing compound and with $a=5.5088(1)$ Å; $b=5.6226(1)$ Å; $c=7.8601(1)$ Å; $\beta=90.02(1)^\circ$ for Ca containing compound. Three phase transitions with temperature are observed in Sr_2ScSbO_6: $P2_1/n \rightarrow I2/m \rightarrow I4/m \rightarrow Fm\bar{3}m$, at about 400, 560 and 650 K, respectively. The large distortion of Ca_2ScSbO_6 at room temperature leads to a higher temperature phase transition from $P2_1/n$ to $I2/m$ at about 1440 K. This fact, it was not possible to observe the other phase transitions to the higher symmetries due to the instrument limitations.

Acknowledgments

This work was done in part under project numbers: UPV 0063.310-13564/2001-2007 and MAT2008-05839/MAT. The authors thank the Hahn-Meitner-Institut (BENSC) for the provision of neutron beamtime and the staff of E9 for their kind help and technical assistance. The authors appreciate and thank very much the remarks and comments made by the referees, which have improve the manuscript.

References

[1] K.-I. Kobayashi, T. Kimura, H. Sawada, K. Terakura, Y. Tokura, Nature 395 (1998) 677–680.
[2] M. DeMarco, H.A. Blackstead, J.D. Dow, M.K. Wu, D.Y. Chen, E.Z. Chien, H. Haka, S. Toorongian, J. Fridmann, Phys. Rev. B 62 (2000) 14301–14303.
[3] E.J. Cussen, J.F. Vente, P.D. Battle, T.C. Gibb, J. Mater. Chem. 7 (1997) 459–463.
[4] N. Kashima, K. Inoue, T. Wada, Y. Yamaguchi, Appl. Phys. A 74 (2002) S805–S807.
[5] H. Karunadasa, Q. Huang, B.G. Ueland, P. Schiffer, R.J. Cava, PNAS V 100 (2003) 8097–8102.
[6] V. Primo-Martín, M. Jansen, J. Solid State Chem. 157 (2001) 76–85.
[7] A. Tauber, S.C. Tidow, R.D. Finnegan, W.D. Wilber, Physica C 256 (1996) 340–344.
[8] W.T. Fu, D.J.W. Ijdo, Solid State Commun. 134 (2005) 177–181.
[9] M.W. Lufaso, R.B. Macquart, Y. Lee, T. Vogt, H.C. Loye, J. Phys. Condens. Matter 18 (2006) 8761–8780.
[10] S.A. Ivanov, P. Nordblad, R. Tellgren, A. Hewat, Mater. Res. Bull. 44 (2009) 822–830.
[11] C. Bharti, T.P. Sinha, Solid State Sci. V 12 (2010) 498–502.
[12] A. Faik, M. Gateshki, J.M. Igartua, J.L. Pizarro, M. Insausti, R. Kaindl, A. Grzechnik, J. Sol. State Chem. V 181 (2008) 1759–1766.
[13] A. Faik, E. Iturbe-Zabalo, I. Urcelay, J.M. Igartua, J. Sol. State Chem. V 182 (2009) 2656–2663.
[14] A. Faik, J.M. Igartua, M. Gateshki, G.J. Cuello, J. Sol. State Chem. V 182 (2009) 1717–1725.
[15] A. Faik, J.M. Igartua, E. Iturbe-Zabalo, G.J. Cuello, J. Mol. Struct. 963 (2010) 145–152.
[16] A. Faik, I. Urcelay, E. Iturbe-Zabalo, J.M. Igartua, J. Mol. Struct. 977 (2010) 137–144.
[17] V.V. Wittmann, G. Rauser, S. Kemmier-Sack, Z. Anorg. Allg. Chem. 482 (1981) 143.
[18] J. Rodríguez-Carvajal, Physica B 192 (1993) 55–69.
[19] R.D. Shannon, Acta Cryst. A 32 (1976) 751.
[20] A.M. Glazer, Acta Cryst. B 28 (1972) 3384–3392;
A.M. Glazer, Acta Cryst. A 31 (1975) 756–762.
[21] C.J. Howard, B.J. Kennedy, P.M. Woodward, Acta Cryst. B 59 (2003) 463–471.
[22] D. Orobengoa, C. Capillas, M.I. Aroyo, J.M. Perez-Mato, J. Appl. Cryst. A 42 (2009) 820–833.
[23] D. Orobengoa, J. Rodríguez-Carvajal, J.M. Perez-Mato, M.I. Aroyo, A. Faik, J.M. Igartua, Acta Cryst. A 65 (2009) s328.
[24] J.M. Perez-Mato, D. Orobengoa, M.I. Aroyo, Acta Cryst. A 66 (2010) 558–590.
[25] C. Capillas, E. Kroumova, M.I. Aroyo, J.M. Perez-Mato, H.T. Stokes, D.M. Hatch, J. Appl. Cryst. 36 (2003) 953–954.